Electronic Supporting Information

The electron that breaks the catalyst's back — excited state dynamics in intermediates of molecular photocatalysts

Carolin Müller,[a,b] Ilse Friedländer,[a] Benedikt Bagemihl,[c] Sven Rau,[c] and Benjamin Dietzek*[a,b,d]

[a] Friedrich Schiller University Jena, Helmholtzweg 4, 07743 Jena, Germany, E-mail: benjamin.dietzek@uni-jena.de; Fax: +49-3641-948302; Tel: +49-3641-948360
[b] Leibniz Institute of Photonic Technologiy (Leibniz-IPHT) e.V., Functional Interfaces, Albert-Einstein-Straße 9, 07745 Jena, Germany
[c] Institute of Inorganic Chemistry I, Ulm University, Albert-Einstein-Allee 11, 89081, Ulm, Germany
[d] Friedrich Schiller University Jena, Center for Energy and Environmental Chemistry Jena (CEEC Jena), Lessingstraße 8, 07743 Jena, Germany

Contents

1 UVvis-absorption spectroelectrochemistry

The UVvis absorption spectra of electrochemically generated singly-reduced species of Ru-tpphz-PtI_2 and ^{F}Ru-tpphz-PtI_2 and their mono-metallic precursor complexes – Ru-tpphz and ^{F}Ru-tpphz – were run on a fiber-spectrophotometer (AVANTES). Cyclic voltammograms were obtained using a VersaStat potentiostat. The electrochemical and spectroelectrochemical (SEC) measurements were carried out under nitrogen atmosphere (inside a glovebox) using a thin-layer quartz glass SEC cell (1 mm path length, Bioanalytical Systems, Inc.) equipped with three-electrodes: a platinum counter electrode, a $Ag^{0/+}$ pseudo-reference electrode and a custom-made glassy carbon working electrode with a U-shape hole allowing transmission mode measurements. The measurements were performed in acetonitrile (Aldrich, HPLC-grade) which was dried over calcium hydride prior to use. Solutions of the bi-metallic complexes Ru-tpphz-PtI_2 (0.5 mM) and ^{F}Ru-tpphz-PtI_2 (0.4 mM) as well as of the mono-metallic reference systems Ru-tpphz (0.1 mM) and ^{F}Ru-tpphz (0.2 mM) containing 0.1 M tetrabutylammonium tetrafluoroborate (n-Bu_4NBF_4, Sigma Aldrich for electrochemical analysis, $\geq$99.0 %) as supporting electrolyte were used. Ferrocene/Ferrocenium ($Fc^{0/+}$) was used as an internal standard in the electrochemical measurements. For the UVvis spectroelectrochemical measurements, the reduced species was generated at the glassy carbon electrode by applying a fixed potential (chronoamperometry) for *circa* 2 minutes, while simultaneously UVvis absorption spectra were collected in transmission mode every 20 seconds.

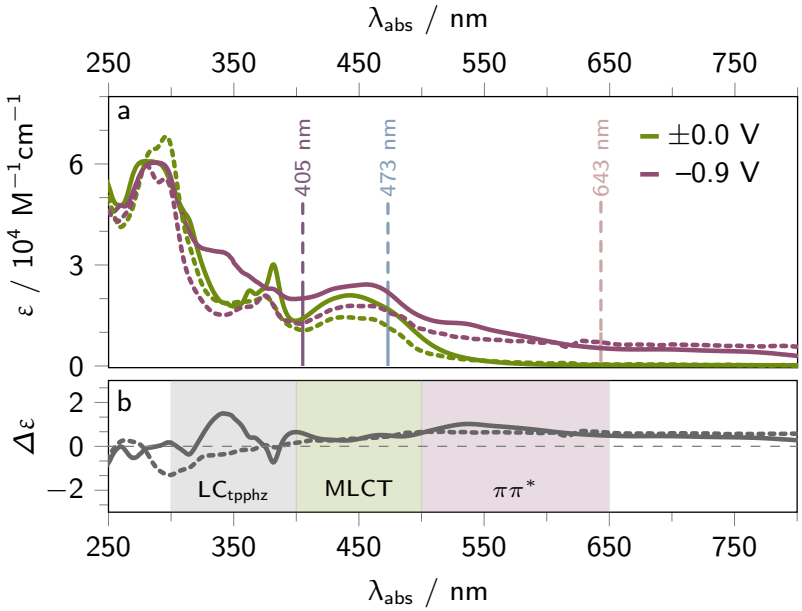

Figure S 1: UVvis absorption spectra (a) of Ru-tpphz (solid, green line) and ^{F}Ru-tpphz (dashed, green line) and their singly-reduced forms, Ru-tpphz$^{\bullet-}$ (solid, violet line) and ^{F}Ru-tpphz$^{\bullet-}$ (dashed, violet line), in acetonitrile. The singly-reduced species were formed upon electrolysis for 1 min at –0.9 V *vs.* $Ag^{0/+}$ in the presence of 0.1 M *n*-Bu_4NBF_4. The difference spectra (b) of Ru-tpphz$^{\bullet-}$ (solid, grey line) and ^{F}Ru-tpphz$^{\bullet-}$ (dashed, grey line) are obtained by subtraction of the respective parental spectrum (green lines, top).

A detailed description of the absorption changes of Ru-tpphz upon single-electron reduction can be found elsewhere.[Zedler2014] Briefly, upon forming Ru-tpphz$^{\bullet-}$ from Ru-tpphz new absorption

features arise between 450 and 750 nm and between 320 and 380 nm. Those features are associated with reduction induced intraligand $\pi\pi^*$ transitions on the tpphz-ligand, where electron density is redistributed from the phz towards the phen moieties of the tpphz ligand. Moreover, single electron reduction causes an increase of the Ru-to-tbbpy with respect to Ru-to-tpphz MLCT transitions, which is reflected in the red-shift of the MLCT absorption maximum. Similar spectral changes are found for ^{F}Ru-tpphz upon electrochemical single-electron reduction forming ^{F}Ru-tpphz$^{\bullet-}$ (see Figure 1). This indicates that the first reduction occurs on the tpphz ligand, although the trifluormethyl-substituents stabilize the bipyridyl-type acceptor orbitals compared to them in Ru-tpphz.

2 Resonance Raman spectroelectrochemistry

The *in situ* resonance Raman (rR) spectroelectrochemical measurements were recorded in transmission mode, using a 1 mm quartz cell equipped with three electrodes: a platinum wire counter electrode, a $Ag^{0/+}$ reference electrode and a glassy carbon working electrode with a hole (1 mm diameter). As excitation light sources a 405 nm diode laser (TopMode-405-HP, Toptica), a 473 nm diode pumped solid-state laser (HB-Laser) and a 643 nm laser were used. After the excitation light passed through a clean-up filter (Semrock) it was focused on the sample solution (1 mm cuvette). To prevent the detection of the excitation- and Rayleigh scattered light in transmission mode, the scattered light subsequently passes through a long-pass filter (>405 nm, >473 nm, or >647 nm, Semrock) and is finally collected by a spectrometer (IsoPlane 160, Princeton Instruments) with an entrance slit of 0.05 mm, at a focal length of 7.5 cm and a grating with 1200 lines per 1 mm (λ_{exc} = 405 and 473 nm) or 600 lines per 1 mm (λ_{exc} = 643 nm). The Raman signals are recorded by a thermoelectrically cooled camera (Pixis eXcelon, Princeton Instruments).

The rR measurements were performed on solutions of Ru-tpphz-PtI_2 (0.4 mM), ^{F}Ru-tpphz-PtI_2 (0.4 mM), Ru-tpphz (0.2 mM) and ^{F}Ru-tpphz (0.2 mM) in acetonitrile containing 0.1 M tetrabutylammonium tetrafluoroborate (n-Bu_4NBF_4, Sigma Aldrich for electrochemical analysis, ≥99.0 %) as supporting electrolyte. Cyclic voltammograms were obtained using a BioLogic SP-50 potentiostat. The singly-reduced species were generated at the glassy carbon working electrode upon electrolysis at –1.3 V *vs.* $Fc^{0/+}$ (chronoamperometry) for 10 minutes. The respective rR spectra between 900 and 2500 relative wavenumbers (rel. $\tilde{\nu}$ cm^{-1}) were collected at a laser power of 5 mW (λ_{exc} = 405 and 473 nm) or 10 mW (λ_{exc} = 643 nm) every 2 minutes (exposure time of 2 seconds with 60 accumulations).

A detailed discussion of the rR data of Ru-tpphz and Ru-tpphz$^{\bullet-}$ collected upon 458 and 514 nm excitation can be found in literature.[**Zedler2014**, **Tschierlei2009b**] Briefly, upon excitation between 400 and 500 nm dominantly, vibrations of the terminal tbbpy and tpphz ligand are observed, indicating an initial excitation of both Ru-to-tbbpy and Ru-to-tpphz MLCT transitions. Upon single-electron reduction this MLCT ratio is shifted towards the bipyridyl sphere, which is revealed in the rR spectra collected upon 405 and 473 nm (see Figure 2). At 643 nm excitation, exclusively tpphz associated rR modes are obtained for the singly-reduced forms, indicating that the first reduction is localized on that ligand sphere.

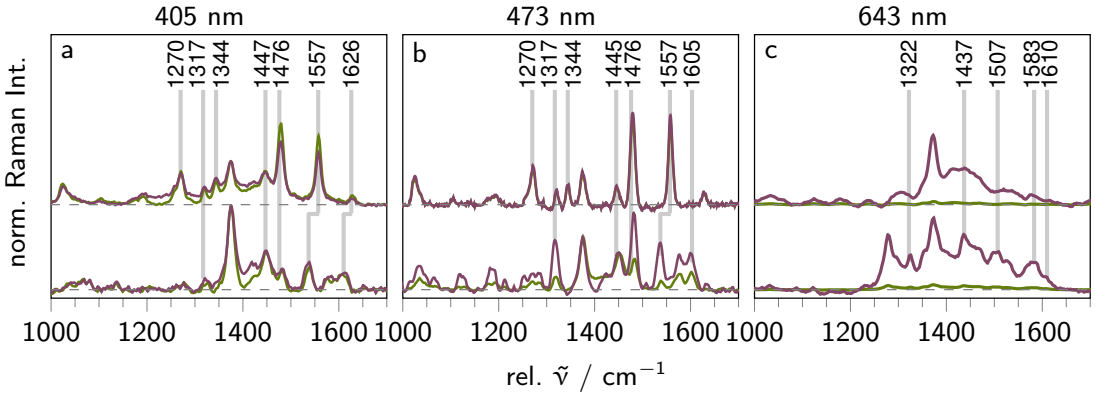

Figure S 2: (Resonance) Raman (rR) spectra of Ru-tpphz (green, bottom) and ^{F}Ru-tpphz (green, top) and upon single-electron reduction (violet spectra) in acetonitrile collected at 405 nm (a), 473 nm (b), and 643 nm (c) excitation. The singly-reduced species were formed upon electrolysis for 1 min at –1.1 V *vs.* $Fc^{0/+}$. All spectra are normalized to the solvent band at 1373 cm^{-1}.

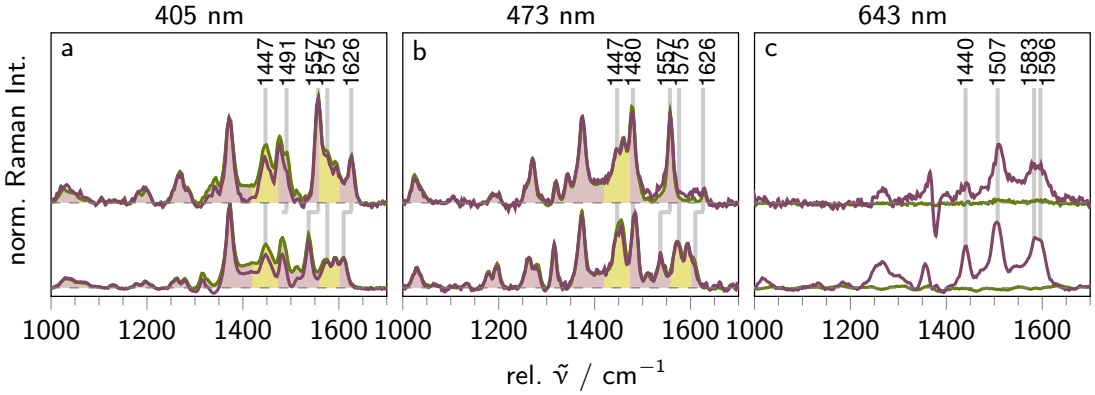

Figure S 3: (Resonance) Raman (rR) spectra of Ru-tpphz-PtI_2 (green, bottom) and ^{F}Ru-tpphz-PtI_2 (green, top) and upon single-electron reduction (violet spectra) in acetonitrile collected at 405 nm (a), 473 nm (b), and 643 nm (c) excitation. The singly-reduced species were formed upon electrolysis for 1 min at –1.3 V *vs.* $Fc^{0/+}$. The colors in the rR spectra indicate tbbpy/dtfmbpy (red) and tpphz (yellow) associated modes. At 643 nm excitation, exclusively tpphz associated rR modes are obtained for the singly-reduced forms, indicating that the first reduction is localized on that ligand sphere. All spectra are normalized to the solvent band at 1373 cm^{-1}.

3 Ultrafast Transient Absorption (fs-TA) Spectroscopy

The ultrafast transient absorption setup is based on a titanium-doped sapphire (Ti:Sa) laser (Legend-Elite, Coherent inc.), which produces pulses centered at 795 nm with a pulse duration 100 fs and pulse energies >1 mJ at a repetition rate of 1 kHz. The 400 nm excitation pump-pulses were generated by second harmonic generation using a BBO crystal. The pump-pulses centered at 580 nm were generated in a collinear optical parametric amplifier (TOPAS-C, LightConversion Ltd.). The pump-pulses are focused (lens, f=80 cm) on the sample with an intensity of about 0.4 mW and a gaussian beam profile of *circa* 400 × 400 μm (400 nm) or 500 × 500 μm (580 nm) at the sample

position. White-light was used for probing the photoinduced dynamics. To generate the white probe-light, part of the 795 nm fundamental beam was focused into a concentrically rotating CaF_2-plate. The probe-pulses were delayed with respect to the arrival of the pump-pulses at the sample position by means of an optical delay stage (maximum delay of 2 ns). The supercontinuum-pulses were split into trains of probe and reference pulses. While the reference-pulses are directly focused onto a diode array detector, the probe-pulses were focused onto the sample by a concave mirror (f=500 mm). The probe- and pump-pulses are spatially and temporally overlapped at the sample position. The relative polarization of the pump- and the probe-pulses were set to magic-angle configuration (54.7°) using a Berek compensator and a polarizer. After passing through the sample, the probe-pulses are recollimated and spectrally dispersed by a prism into probe wavelengths and detected by a diode array (Pascher Instruments, AB). The diode array is read out with the laser repetition rate. A chopper in the pump-path is used to block every second pump (500 Hz repetition rate), such that the signal ΔA(Δt) can be calculated from the two consecutive probe-pulses corresponding to the pump-on (I_p) and pump-off (I_0) conditions according to

$$\Delta A(\Delta t, \lambda) = -\lg\left(\frac{I_p(\Delta t, \lambda) - I_0(\lambda)}{I_0(\lambda)}\right) \tag{1}$$

3.1 fs-TA data of ^{F}Ru-tpphz and ^{F}Ru-tpphz-PtI$_2$ in acetonitrile

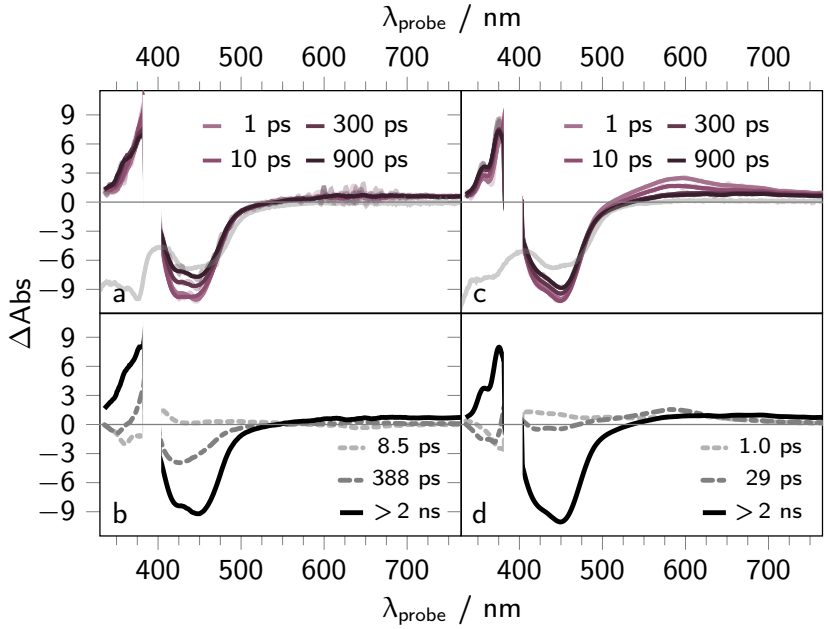

Figure S 4: Transient absorption (top row) and decay associated spectra (bottom row) of ^{F}Ru-tpphz (a and b) and ^{F}Ru-tpphz-PtI$_2$ (c and d) upon 400 nm excitation in acetonitrile. For comparison, the inverted steady-state absorption spectra of ^{F}Ru-tpphz and ^{F}Ru-tpphz-PtI$_2$ are shown (gray) and scaled to the largest ground-state bleach signal (a and c).

3.2 fs-TA Spectroelectrochemistry

The fs-TA electrochemical measurements, *i.e.*, the cyclic voltammograms and chronoamperometry curves and transient spectra at an applied potential were obtained using a PASCHER INSTRUMENT with an in-built potentiostat. The spectroelectrochemical measurements were performed in the same custom-built cell as used for the resonance Raman measurements, *i.e.*, a quartz cell (1 mm path length) equipped with a platinum wire counter electrode, a $Ag^{0/+}$ pseudo-reference electrode and a glassy carbon working electrode. The spectra are collected in transmission mode (pump and probe beam are allowed to go through a 1 mm hole in the glassy carbon electrode). The experiments were performed at a sample concentration of around 0.4 mM and the presence of supporting electrolyte (0.1 M n-Bu_4NBF_4). The solutions were prepared under argon atmosphere and prior to each measurement the cell was purged with argon for about one minute. The reduced species were generated at the glassy carbon electrode by applying a fixed potential (chronoamperometry). To make sure that a comparable high concentration of reduced species are formed, a chronoamperometry curve and the corresponding absorption spectra (transmitted white light) were collected simultaneously. Once, the absorption changes and current are stable (after 2 to 5 minutes of electrolysis) the fs-TA spectra were monitored (see above).

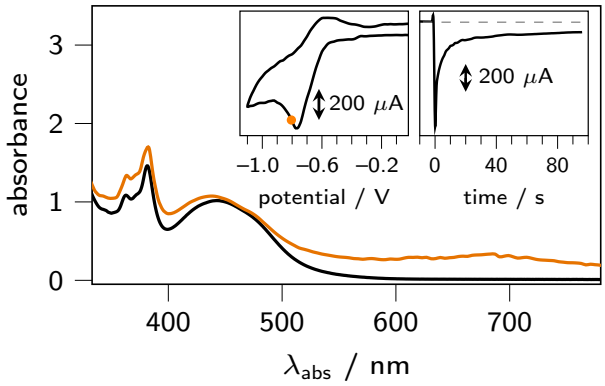

Figure S 5: UVvis absorption spectra of Ru-tpphz in acetonitrile (black line) and upon single-electron reduction (orange line). The insets show the cyclic voltammogram (CV) and chronoamperometry (CA) curves collected in the transient absorption spectroelectrochemical cell. In the CV curve the applied reduction potential is highlighted. The formation of the reduced complex is displayed at that potential in the CA curve. The reduction was performed in the presence of 0.1 M *n*-Bu_4NBF_4. The reduction potential is measured *vs.* a Ag/Ag^+ electrode.

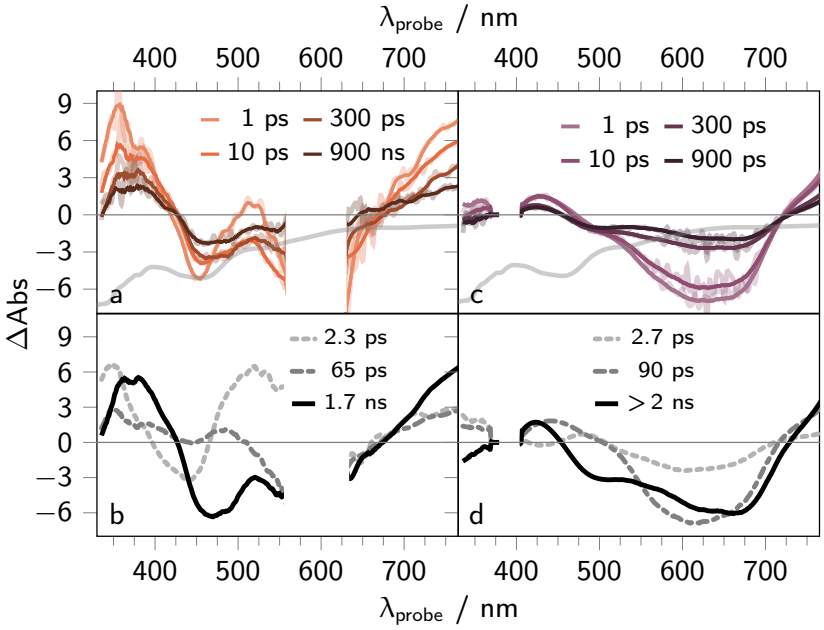

Figure S 6: Transient absorption (a and c) and decay associated spectra (b and d) of Ru-tpphz$^{\bullet-}$ upon 590 nm (a and b, 0.4 mW) and 400 nm excitation (c and d, 0.5 mW) in acetonitrile. For comparison, the inverted steady-state absorption spectrum of Ru-tpphz$^{\bullet-}$ is shown (gray) and scaled to the largest ground-state bleach signal at 590 nm (a and c). The reduced photocatalyst was electrochemically formed at a glassy carbon electrode (−0.8 V *vs.* $Ag^{0/+}$, 0.1 M n-Bu_4NBF_4).

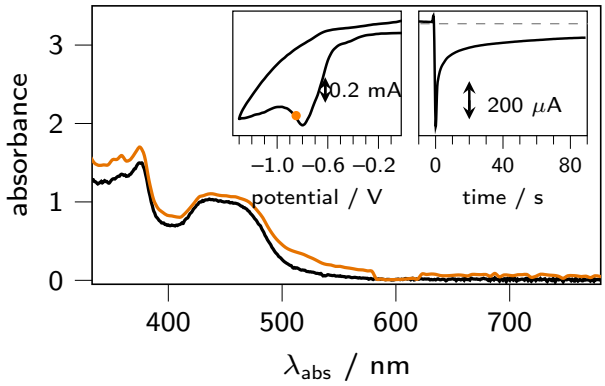

Figure S 7: UVvis absorption spectra of ^{F}Ru-tpphz in acetonitrile (black line) and upon single-electron reduction (orange line). The insets show the cyclic voltammogram (CV) and chronoamperometry (CA) curves collected in the transient absorption spectroelectrochemical cell. In the CV curve the applied reduction potential is highlighted. The formation of the reduced complex is displayed at that potential in the CA curve. The reduction was performed in the presence of 0.1 M *n*-Bu_4NBF_4. The reduction potential is measured *vs.* a Ag/Ag^+ electrode.

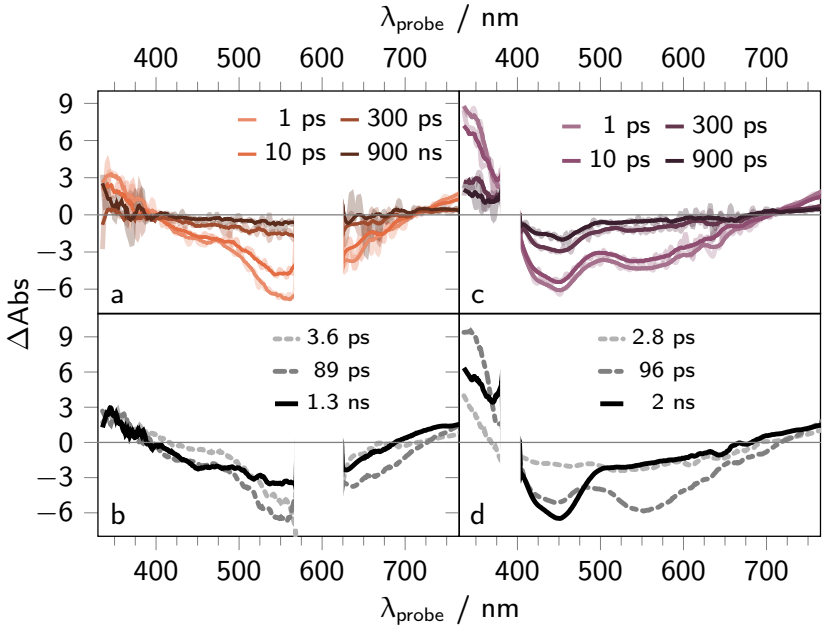

Figure S 8: Transient absorption (a and c) and decay associated spectra (b and d) of ^{F}Ru-tpphz$^{\bullet-}$ upon 590 nm (a and b, 0.4 mW) and 400 nm excitation (c and d, 0.5 mW) in acetonitrile. For comparison, the inverted steady-state absorption spectrum of ^{F}Ru-tpphz$^{\bullet-}$ is shown (gray) and scaled to the largest ground-state bleach signal at 590 nm (a and c). The reduced photocatalyst was electrochemically formed at a glassy carbon electrode (−0.85 V *vs.* $Ag^{0/+}$, 0.1 M n-Bu_4NBF_4).

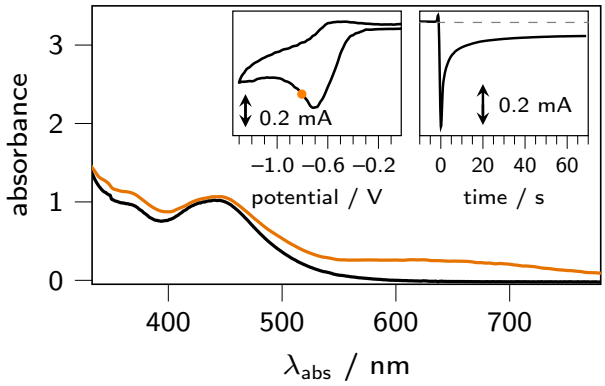

Figure S 9: UVvis absorption spectra of Ru-tpphz-PtI_2 in acetonitrile (black line) and upon single-electron reduction (orange line). The insets show the cyclic voltammogram (CV) and chronoamperometry (CA) curves collected in the transient absorption spectroelectrochemical cell. In the CV curve the applied reduction potential is highlighted. The formation of the reduced complex is displayed at that potential in the CA curve. The reduction was performed in the presence of 0.1 M *n*-Bu_4NBF_4. The reduction potential is measured *vs.* a Ag/Ag^+ electrode.

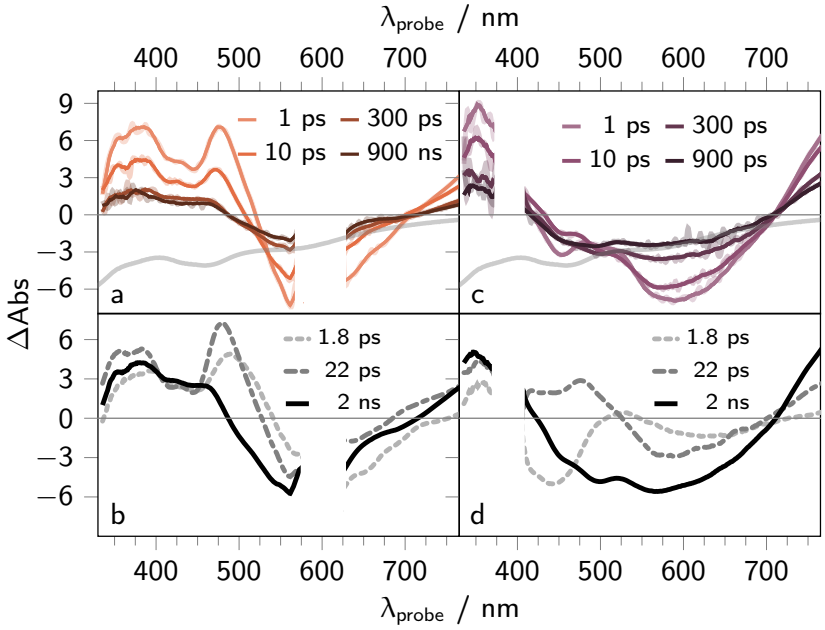

Figure S 10: Transient absorption (a and c) and decay associated spectra (b and d) of Ru-tpphz$^{\bullet-}$-PtI_2 upon 590 nm (a and b, 0.4 mW) and 400 nm excitation (c and d, 0.5 mW) in acetonitrile. For comparison, the inverted steady-state absorption spectrum of Ru-tpphz$^{\bullet-}$-PtI_2 is shown (gray) and scaled to the largest ground-state bleach signal at 590 nm (a and c). The reduced photocatalyst was electrochemically formed at a glassy carbon electrode (−0.95 V *vs.* $Ag^{0/+}$, 0.1 M n-Bu_4NBF_4).

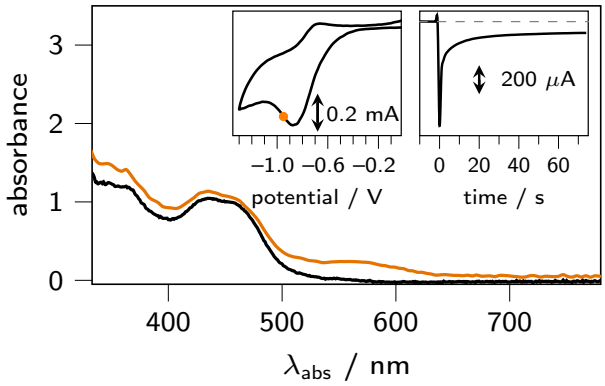

Figure S 11: UVvis absorption spectra of ^{F}Ru-tpphz-PtI$_2$ in acetonitrile (black line) and upon single-electron reduction (orange line). The insets show the cyclic voltammogram (CV) and chronoamperometry (CA) curves collected in the transient absorption spectroelectrochemical cell. In the CV curve the applied reduction potential is highlighted. The formation of the reduced complex is displayed at that potential in the CA curve. The reduction was performed in the presence of 0.1 M *n*-Bu$_4$NBF$_4$. The reduction potential is measured *vs.* a Ag/Ag$^+$ electrode.

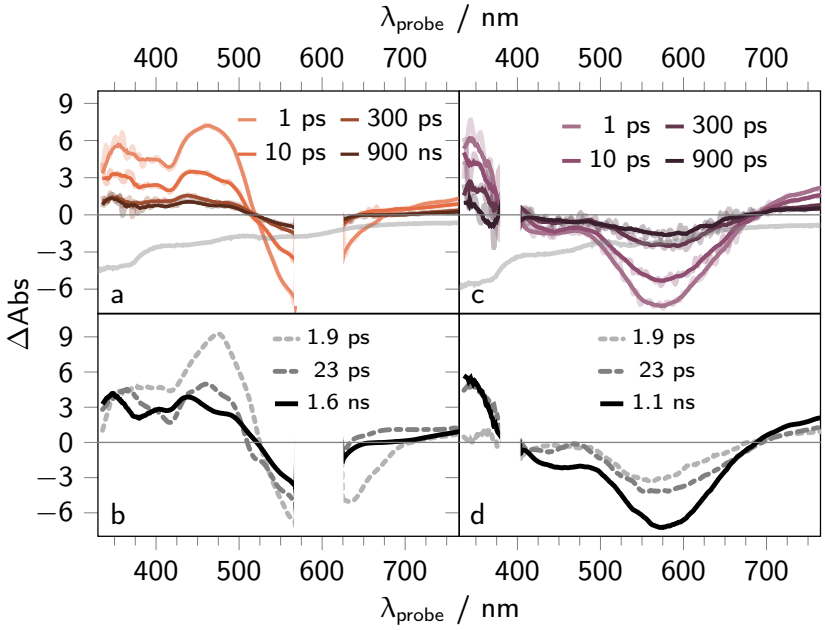

Figure S 12: Transient absorption (a and c) and decay associated spectra (b and d) of ^{F}Ru-tpphz$^{\bullet-}$-PtI$_2$ upon 590 nm (a and b, 0.4 mW) and 400 nm excitation (c and d, 0.5 mW) in acetonitrile. For comparison, the inverted steady-state absorption spectrum of ^{F}Ru-tpphz$^{\bullet-}$-PtI$_2$ is shown (gray) and scaled to the largest ground-state bleach signal at 590 nm (a and c). The reduced photocatalyst was electrochemically formed at a glassy carbon electrode (−0.95 V *vs.* Ag$^{0/+}$, 0.1 M n-Bu$_4$NBF$_4$).

4 Emission Properties

Emission spectroscopy was performed on a JASCO FP-8500 Fluorescence Spectrometer with gas-tight quartz glass cuvettes with a path length of 1 cm. All samples were prepared in a glovebox under argon atmosphere.

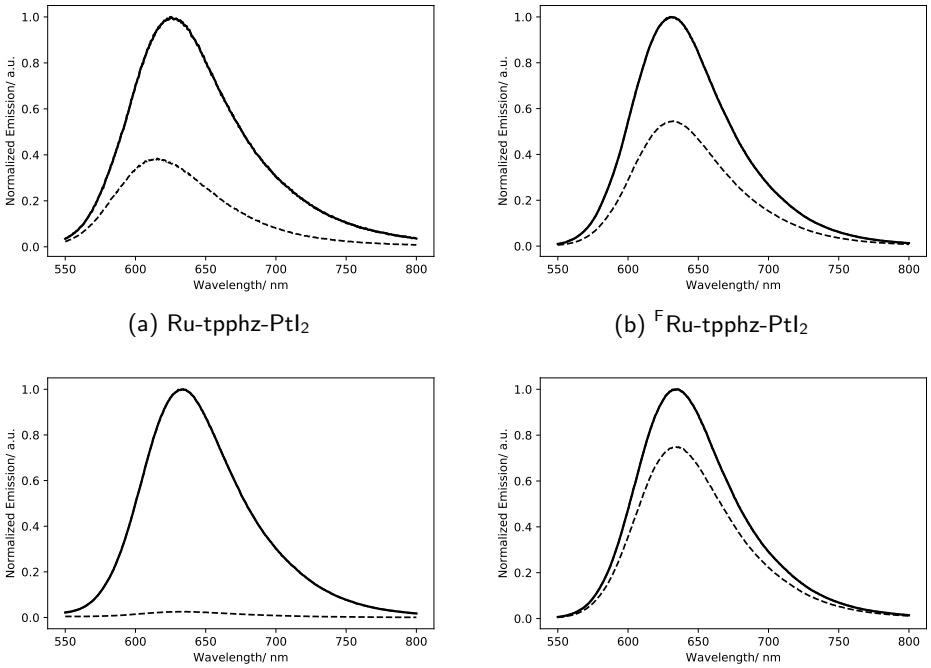

(a) Ru-tpphz-PtI_2 (b) ^{F}Ru-tpphz-PtI_2

(c) Ru-tpphz (d) ^{F}Ru-tpphz

Figure S 13: Emission spectra of Ru-tpphz-PtI_2 and ^{F}Ru-tpphz-PtI_2 and their mono-metallic counterparts Ru-tpphz and ^{F}Ru-tpphz in de-aerated acetonitrile (solid line) and in a de-aerated acetonitrile:water mixture (1:1, *v:v*). The concentration of each complex is kept constant in both solvents.

Luminescence quantum yields were determined by the relative method[1] using the standard Ruthenium-tris(bipyridine) as its hexafluorophosphate salt purchased from Sigma Aldrich. According to the literature the quantum yield of this standard in acetonitrile under an inert atmosphere is 0.095.[2] From a total of four measurements of different concentrations with an optical density below 0.1, the luminescence quantum yield was determined. In Table 1, the averaged values with the respective standard deviations are reported.

Table S 1: Emission quantum yields (QY) of Ru-tpphz-PtI_2 and ^{F}Ru-tpphz-PtI_2 and their mono-metallic counterparts Ru-tpphz and ^{F}Ru-tpphz in de-aerated acetonitrile.

compound	counter-ion	QY / %
Ru-tpphz-PtI_2	2 PF_6^-	0.4±0.1
^{F}Ru-tpphz-PtI_2	2 $BArF^-$	4.8±0.6
Ru-tpphz	2 PF_6^-	7.7±0.5
^{F}Ru-tpphz	2 $BArF^-$	6.7±0.5

5 Synthesis and Characterization

Ru-tpphz-PtI_2 and the monometallic complex Ru-tpphz were synthesized according to literature.[3] Sodium tetrakis[3,5-bis(trifluoromethyl)phenyl]borate (NaBArF),[4] tetrapyrido[3,2-a:2',3'-c:3'',2''-h:2''',3'''-j]phenazine (tpphz)[5] and *cis*-[$Pt(DMSO)_2I_2$] (DMSO = Dimethyl-sulfoxide)[6] were synthesized as previously reported. 4,4'-bis(trifluoromethyl)-2,2'-bipyridine) (fbpy) was purchased from ABCR.

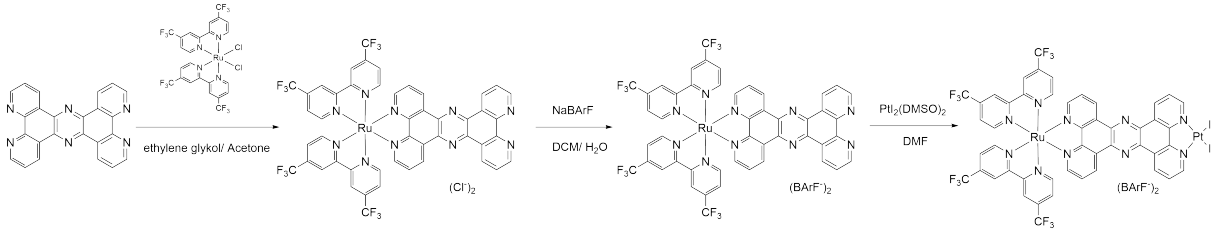

(a) Overview of the synthesis of ^{F}Ru-tpphz-PtI_2 $(BArF)_2$.

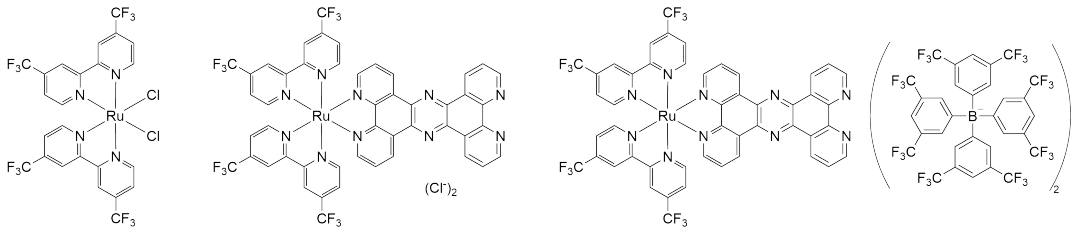

(b) $^{F}RuCl_2$ (c) ^{F}Ru-tpphz Cl_2 (d) ^{F}Ru-tpphz $(BArF)_2$

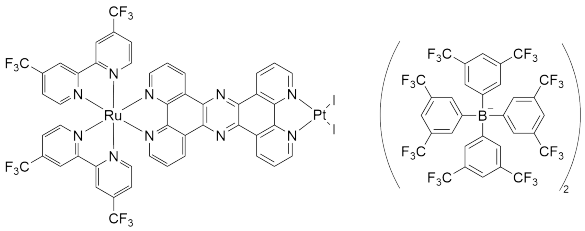

(e) ^{F}Ru-tpphz-$PtI_2(BArF)_2$

Figure S 14: Overview of ruthenium complexes involved in this work.

[Dichlorido-bis(4,4'-bis(trifluoromethyl)-2,2'-bipyridine)ruthenium(II)] ($^{F}RuCl_2$)

This compound has been prepared already in the literature.[7–9] Nevertheless, we found a procedure, which involves only the low boiling-point solvent ethanol, which we think is a benefit compared to previous DMF-based syntheses. Ruthenium chloride hydrate (153 mg, 0.529 mmol, 1.0 eq) was dispersed with 4,4'-bis(trifluoromethyl)-2,2'-bipyridine (312 mg, 1.07 mmol, 2.0 eq) in 50 mL of absolute ethanol. The mixture was heated to reflux for 15 hours. The crude reaction solution was concentrated in vaccuo and filtered through a glass frit. The residue was washed with cold ethanol and diethyl ether and then washed from the frit using chloroform. The solvent was removed and the product dried in high vacuum. Yield (based on Ruthenium content of 37.5% in Ruthenium chloride hydrate): 87% (348 mg, 0.46 mmol).

^{1}**H-NMR** (400 MHz, CD_2Cl_2) δ = 10.4 (d, J = 6.0 Hz, 2H), 8.5 (s, 2H), 8.4 (s, 2H), 7.9 (dd, J = 6.0, 1.8 Hz, 2H), 7.8 (d, J = 6.0 Hz, 2H), 7.3 (dd, J = 6.1, 1.9 Hz, 2H).

^{19}**F-NMR** (376 MHz, CD_2Cl_2) δ = -64.7, -65.0.

[Ruthenium(4,4´-bis(trifluoromethyl)-2,2´-bipyridine)$_2$(tpphz)] dichloride (^{F}Ru-tpphz Cl_2)

A synthesis route derived from Rau *et al.* was used.[10] [Ruthenium(4,4´-bis(trifluoromethyl)-2,2´-bipyridine)$_2$(tpphz)] dichloride (^{F}Ru-tpphz (Cl_2) was synthesized by dispersing tpphz (229 mg, 0.596 mmol, 5 eq.) in 200 mL of ethylene glycol at 180°C. $^{F}RuCl_2$ (90 mg, 0.119 mmol, 1 eq.) was dissolved in a mixture of 20 mL Acetone and 60 mL ethylene glycol in a dropping funnel and added over the course of several hours to the stirring tpphz dispersion. After the addition was completed, the mixture was continued to stir at 180°C for one more hour, before the solvent was removed by distillation under reduced pressure using a water jet pump. The residue of the distillation was taken up using 20 mL of methanol and the resulting solution filtered through a pad of Celite, when excess of tpphz was removed. The solvent of the filtrate was removed by rotary evaporation and the crude product purified *via* size exclusion chromatography (Sephadex LH-20, eluent: methanol) or fractionized crystallization (slow evaporation of methanol from a methanol/ toluene mixture) obtaining a red-orange product in 34% (46 mg, 0.040 mmol) to 54% (73 mg, 0.064 mmol) yield.

^{1}**H-NMR** (500 MHz, MeOD) δ 9.6 (d, J = 9.2 Hz, 2H), 9.5 (d, J = 8.1 Hz, 2H), 9.4 (d, J = 15.8 Hz, 4H), 8.6 (d, J = 6.0 Hz, 2H), 8.4 (dd, J = 28.8, 5.5 Hz, 4H), 8.4 (d, J = 3.4 Hz, 2H), 8.1 (dd, J = 8.2, 5.3 Hz, 2H), 8.0 (d, J = 6.0 Hz, 2H), 7.9 (d, J = 6.1 Hz, 2H), 7.8 (dd, J = 8.1, 4.3 Hz, 2H).

^{13}**C-NMR** (126 MHz, MeOD) δ = 159.8, 159.1, 156.4, 155.5, 155.3, 153.6, 150.7, 148.4, 141.6, 140.9 (q, J = 35.5 Hz), 140.5 (q, J = 35.5 Hz), 139.7, 136.1, 135.2, 131.2, 129.0, 127.4, 126.3, 125.9, 125.4, 125.4, 124.8, 124.8, 124.8, 124.8, 123.7 (qd, J = 273.3, 7.8 Hz), 123.1, 122.8, 120.5, 120.4.

^{19}**F-NMR** (376 MHz, MeOD) δ = -65.9, -66.0.

A portion of the complex was precipitated as its hexafluorophosphate salt using ammonium hexafluorophosphate. The resulting salt was found only hardly soluble in most organic solvents except for DMF and DMSO, which is why the BArF- salt was used for most experiments.

HRMS (MALDI, from PF_6^- salt): [M-2PF_6^-]+ 1070.1045 (calculated: 1070.1037), [M-PF_6^-]+ 1215.0692 (calculated: 1215.0685)

[Ruthenium(4,4´-bis(trifluoromethyl)-2,2´-bipyridine)$_2$(tpphz)] di-(tetrakis[3,5-bis(trifluoromethyl)phenyl] borate) (^{F}Ru-tpphz $BArF_2$)

$BArF^-$ was used as an anion to enhance solubility, as it has been done elsewhere for (flourous) metal complexes.[11–13] For the anion metathesis from chloride to tetrakis[3,5-bis(trifluoromethyl)phenyl] borate ($BArF^-$), a simple extraction procedure was used. Typically, ^{F}Ru-tpphz (Cl_2) (30 mg, 0.026 mmol, 1 eq.) was dissolved with NaBArF (47.3 mg, 0.0533 mmol, 2.05 eq.) in 15 mL of dichloromethane and 25 mL of de-ionized water was added. The mixture was shaken for two minutes, forming an orange emulsion. The emulsion was allowed to break in two phases overnight and the bottom red-orange organic phase was separated and passed through a pad of neutral alumina. The solvent was evaporated yielding 92% (67 mg, 0.024 mmol) of product. The success of the exchange of the anion was ensured *via* ^{1}H-NMR spectroscopy.

^{1}**H-NMR** (400 MHz, Methanol-d_4) δ = 10.0 (s, 2H), 9.9 (s, 2H), 9.4 (d, J = 11.8 Hz, 4H), 9.1 (bs, 2H), 8.4 (d, J = 5.1 Hz, 2H), 8.3 (d, J = 5.8 Hz, 2H), 8.3 – 8.2 (m, 2H), 8.1 (dd, J = 8.2, 5.4 Hz, 2H), 8.1 – 8.0 (m, 2H), 8.0 – 7.9 (m, 2H), 7.7 (d, J = 5.9 Hz, 2H), 7.6 – 7.5 (m, 24H).

^{19}**F-NMR** (376 MHz,Methanol-d_4) δ = −64.3, −66.0, −66.1.

[Ruthenium(4,4´-bis(trifluoromethyl)-2,2´-bipyridine)$_2$(tpphz)platinum(di-iodine)] di-(tetrakis[3,5-bis(trifluoromethyl)phenyl] borate) (^{F}Ru-tpphz-PtI_2 $BArF_2$)

For the coordination of the platinum catalyst, *cis*-[Pt(DMSO)$_2$I$_2$] was used as the source of platinum, but compared to Pfeffer *et al.*,[3] the reaction solvent was changed to dimethyl formamide (DMF) since it allowed to dissolve all reactants more reliably. ^{F}Ru-tpphz ($BArF^-$)$_2$ (39 mg, 0.014 mmol, 1 eq.) was dissolved along with *cis*-[Pt(DMSO)$_2$I$_2$] (10 mg, 0.017 mmol, 1.2 eq) in 10 mL of DMF. The reaction was stirred for 12 hours at 95 °C, after which the solvent of the reaction was removed by rotary evaporation. The crude product was dissolved in dichloromethane, extracted several times against fresh de-ionized water and passed through a plug of neutral alumina, before the solvent was removed to yield the product in 87% (40 mg, 0.012 mmol) yield.

^{1}**H-NMR** (400 MHz, DMSO-d_6) δ = 10.2 (d, J = 6.6 Hz, 1H), 10.1 (d, J = 8.1 Hz, 7H), 10.0 (d, J = 5.5 Hz, 5H), 9.6 (d, J = 8.5 Hz, 26H), 8.4 – 8.3 (m, 23H), 8.3 (d, J = 5.6 Hz, 15H), 8.2 – 8.1 (m, 19H), 8.0 (d, J = 6.4 Hz, 17H), 7.8 (d, J = 6.2 Hz, 7H), 7.7 (s, 76H), 7.6 (s, 171H).

^{19}**F-NMR** (376 MHz, CD_3CN) δ = −63.3, −65.2, −65.3.

HRMS (MALDI): found: [M-2 $BArF^-$]$^+$: 1518.8776 (calculated: 1518.8774), [M-2 $BArF^-$]$^+$: 2381.9437 (calculated: 2381.9429)

5.1 NMR spectra

^{1}H-NMR spectroscopy was performed either on a Bruker Avance 500 MHz or Bruker Avance 400 MHz spectrometer. ^{19}F (376 MHz) and ^{13}C-NMR (126 MHz) spectra were recorded on a Bruker Avance 400 MHz NMR spectrometer. The shift values are given in ppm and are referenced to the corresponding solvent residual peaks.

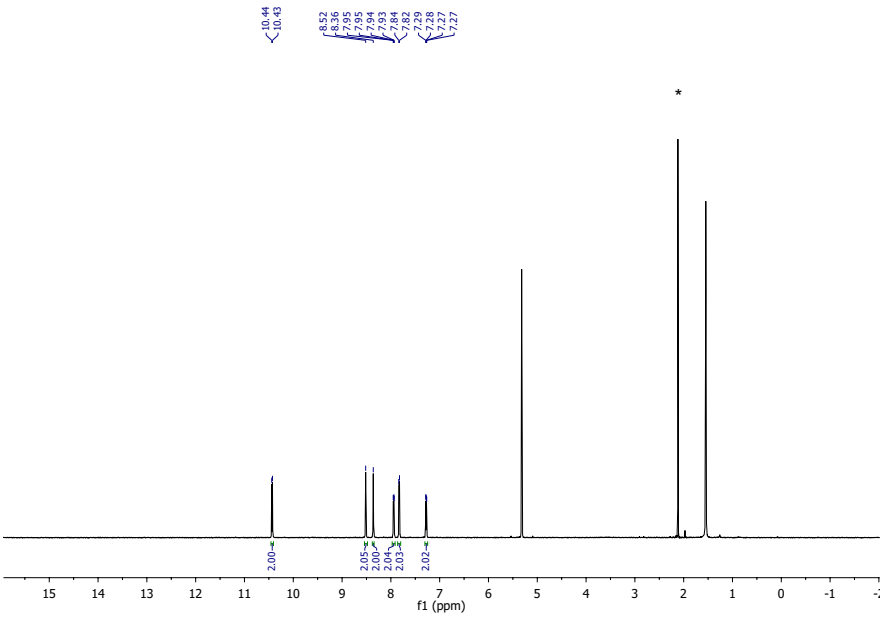

Figure S 15: ^{1}H-NMR spectrum of $^{F}RuCl_2$ in DCM-d_2 (* = residual acetone).

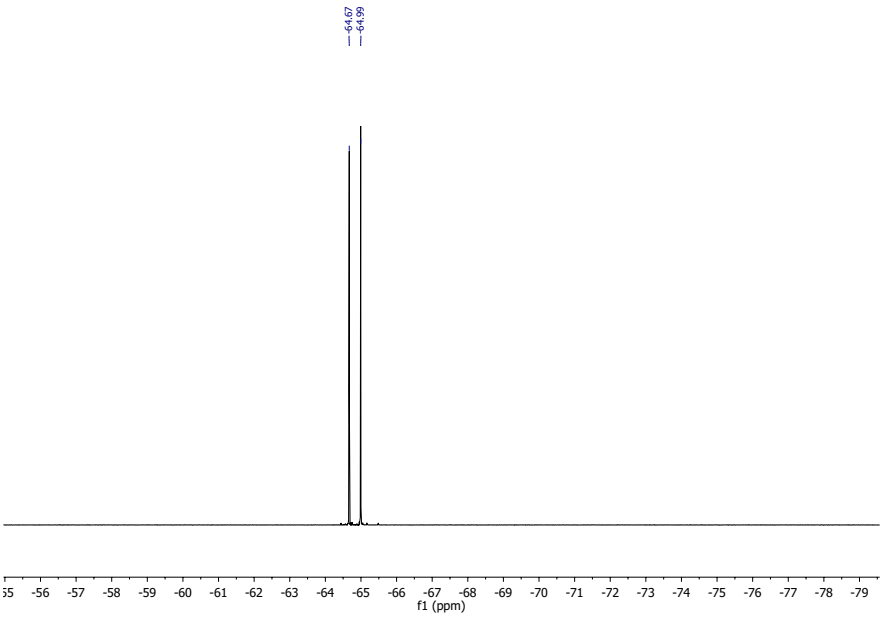

Figure S 16: ^{19}F-NMR spectrum of $^{F}RuCl_2$ in DCM-d_2.

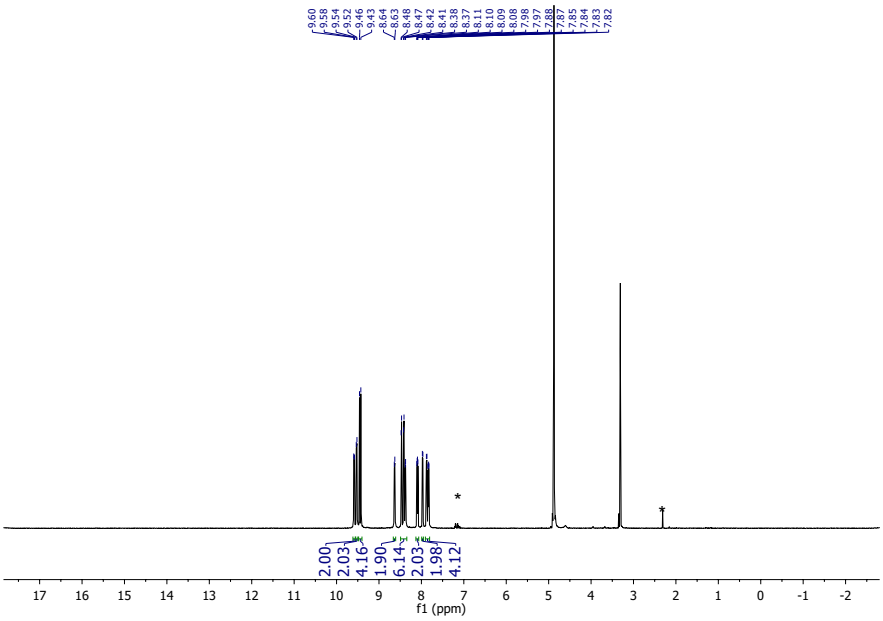

Figure S 17: ^{1}H-NMR spectrum of ^{F}Ru-tpphz Cl_2 in deuterated methanol (* = residual toluene).

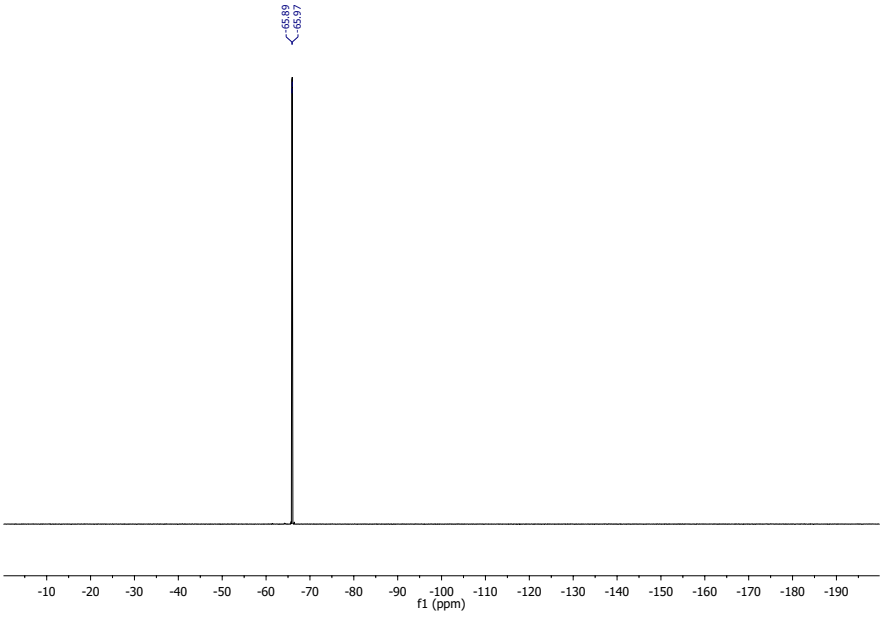

Figure S 18: ^{19}F-NMR spectrum of ^{F}Ru-tpphz Cl_2 in deuterated methanol.

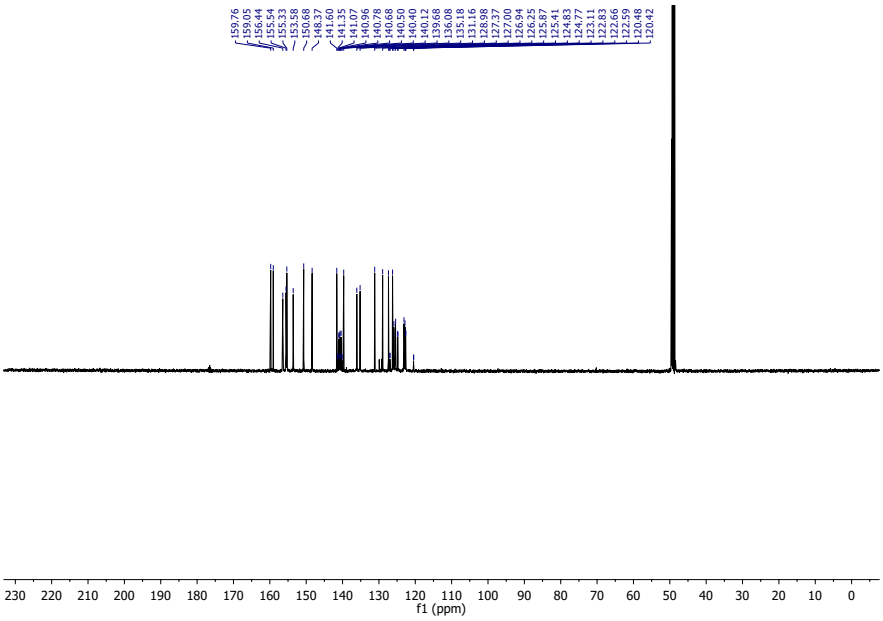

Figure S 19: UDEFT-^{13}C-NMR spectrum of ^{F}Ru-tpphz Cl_2 in deuterated methanol.

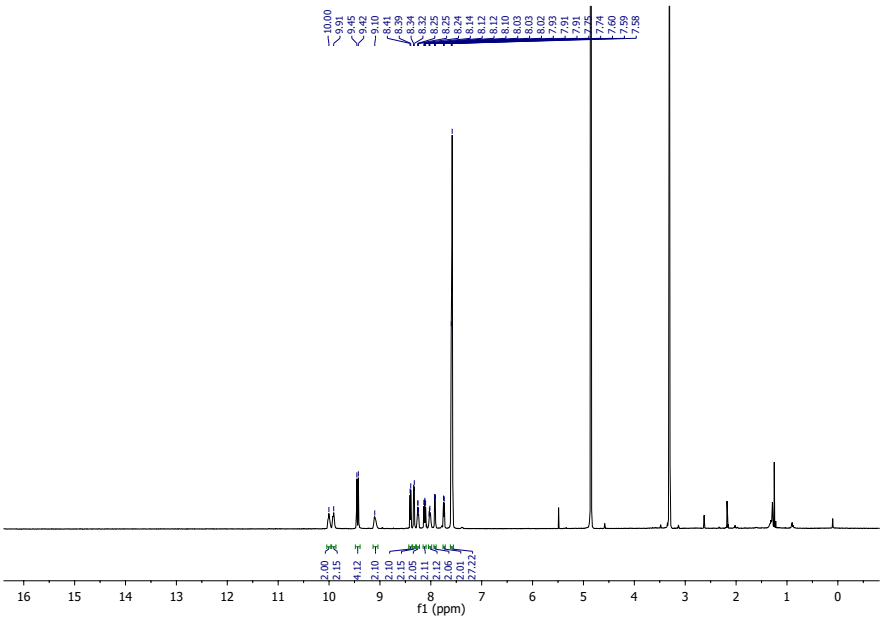

Figure S 20: ^{1}H-NMR spectrum of ^{F}Ru-tpphz $(BArF)_2$ in deuterated methanol.

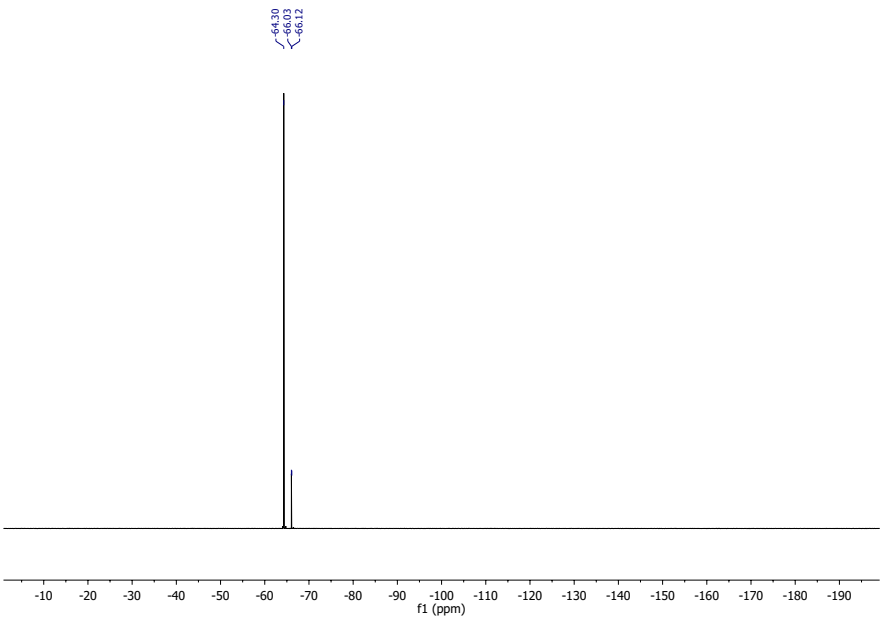

Figure S 21: ^{19}F-NMR spectrum of ^{F}Ru-tpphz $(BArF)_2$ in deuterated methanol.

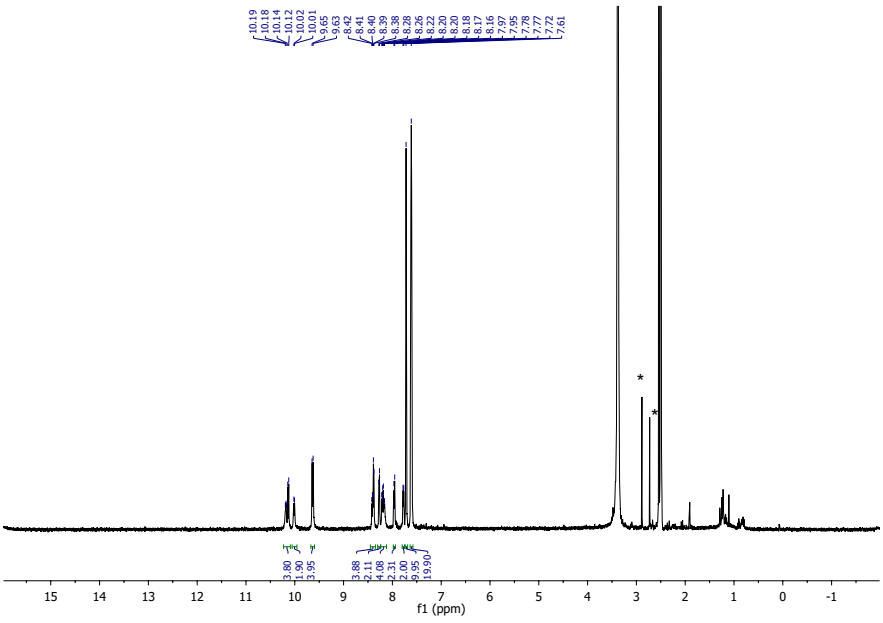

Figure S 22: ^{1}H-NMR spectrum of ^{F}Ru-tpphz-PtI_2 $(BArF)_2$ in DMSO-d_6 (* = residual DMF).

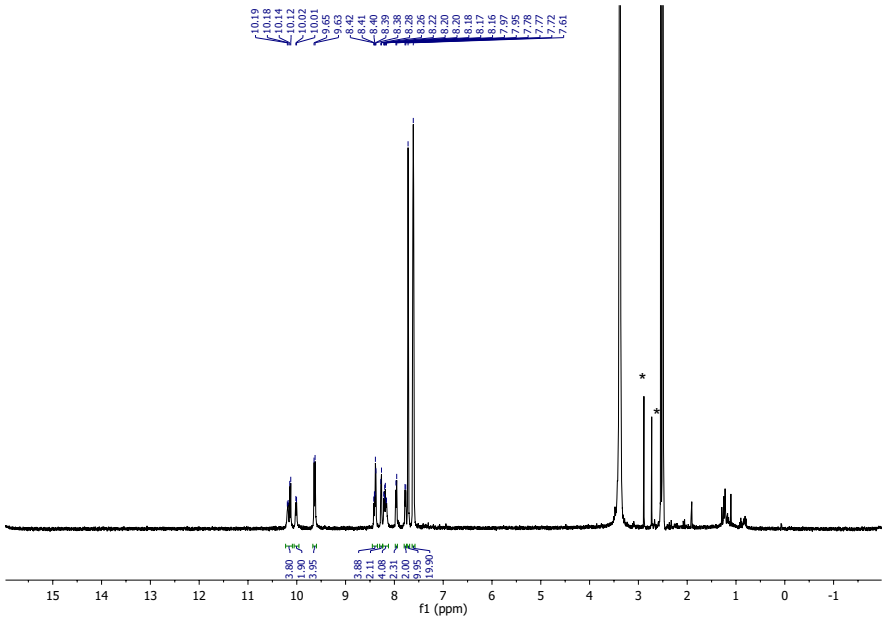

Figure S 23: ^{19}F-NMR spectrum of ^{F}Ru-tpphz-PtI$_2$ (BArF)$_2$ in deuterated acetonitrile.

5.2 HRMS spectra

High resolution mass spectrometry (HRMS) was performed using a Fourier Transform Ion Cyclotron Resonance (FT-ICR) mass spectrometer solariX (Bruker Daltonics) equipped with a 7.0 T superconducting magnet and interfaced to an Apollo II Dual ESI/MALDI source. For all MALDI measurements trans-2-[3-(4-tert-Butylphenyl)-2-methyl-2-propenylidene]malononitrile (DCTB) was used as the matrix. Spectra were analyzed with the DataAnalysisViewer 4.2 from Bruker and transferred to mMass Version 5.5.0.

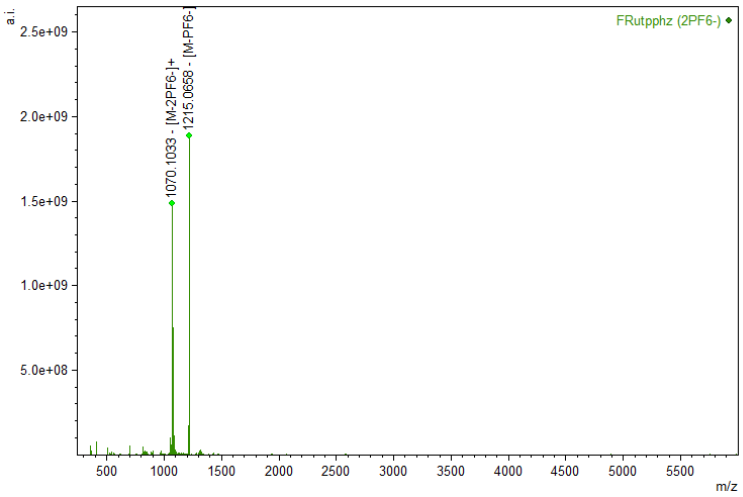

Figure S 24: MALDI-HRMS spectrum of ^{F}Ru-tpphz (PF$_6$)$_2$.

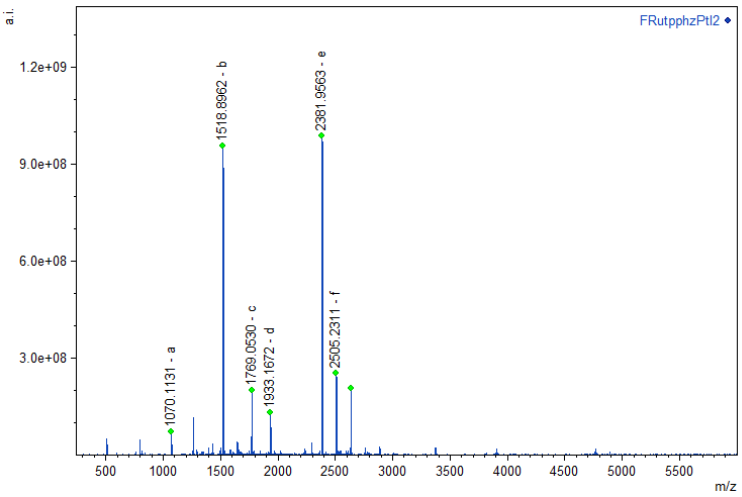

Figure S 25: MALDI-HRMS of ^{F}Ru-tpphz-PtI_2 $(BArF)_2$. a = $[M\text{-}PtI_2\text{-}2BArF^-]^+$; b = $[M\text{-}2BArF^-]^+$, c = $[M\text{-}1BArF^-$ + DCTB$]^+$, d = $[M - PtI_2 - 1BArF^-]^+$, e = $[M - 1BArF^-]^+$, , e = $[M - 1BArF^-$ + DCTB$]$+ where DCTB is the matrix trans-2-[3-(4-tert-Butylphenyl)-2-methyl-2-propenylidene]malononitrile.

References

[1] A. T. R. Williams, S. A. Winfield, J. N. Miller, *Analyst* **1983**, *108*, 1067, DOI 10.1039/an9830801067.

[2] K. Suzuki, A. Kobayashi, S. Kaneko, K. Takehira, T. Yoshihara, H. Ishida, Y. Shiina, S. Oishi, S. Tobita, *Phys. Chem. Chem. Phys.* **2009**, *11*, 9850, DOI 10.1039/b912178a.

[3] M. G. Pfeffer, T. Kowacs, M. Wächtler, J. Guthmuller, B. Dietzek, J. G. Vos, S. Rau, *Angew. Chemie Int. Ed.* **2015**, *54*, 6627–6631, DOI 10.1002/anie.201409442.

[4] N. A. Yakelis, R. G. Bergman, *Organometallics* **2005**, *24*, 3579–3581, DOI 10.1021/om0501428.

[5] J. Bolger, A. Gourdon, E. Ishow, J.-P. Launay, *J. Chem. Soc. Chem. Commun.* **1995**, 1799–1800, DOI 10.1039/C39950001799.

[6] T. Kowacs, L. O'Reilly, Q. Pan, A. Huijser, P. Lang, S. Rau, W. R. Browne, M. T. Pryce, J. G. Vos, *Inorg. Chem.* **2016**, *55*, 2685–2690, DOI 10.1021/acs.inorgchem.5b01752.

[7] R. M. O'Donnell, R. N. Sampaio, G. Li, P. G. Johansson, C. L. Ward, G. J. Meyer, *J. Am. Chem. Soc.* **2016**, *138*, 3891–3903, DOI 10.1021/jacs.6b00454.

[8] J. C. Lennox, J. L. Dempsey, *J. Phys. Chem. B* **2017**, *121*, 10530–10542, DOI 10.1021/acs.jpcb.7b06443.

[9] M. Soler, J. K. McCusker, *J. Am. Chem. Soc.* **2008**, *130*, 4708–4724, DOI 10.1021/ja077096i.

[10] S. Rau, B. Schäfer, D. Gleich, E. Anders, M. Rudolph, M. Friedrich, H. Görls, W. Henry, J. G. Vos, *Angew. Chemie Int. Ed.* **2006**, *45*, 6215–6218, DOI 10.1002/anie.200600543.

[11] B. Guzel, M. A. Omary, J. P. Fackler, A. Akgerman, *Inorganica Chim. Acta* **2001**, *325*, 45–50, DOI 10.1016/S0020-1693(01)00601-6.

[12] T. Harwardt, G. Franciò, W. Leitner, *Chem. Commun.* **2010**, *46*, 6669, DOI 10.1039/c0cc02251a.

[13] T. Achard, L. Egger, C. Tortoreto, L. Guénée, J. Lacour, *Helv. Chim. Acta* **2020**, *103*, e202000190, DOI 10.1002/hlca.202000190.